Journal of Materials Chemistry C

PAPER

View Article Online
View Journal | View Issue

Cite this: J. Mater. Chem. C, 2014, 2, 3416

High-performance two-photon absorption luminophores: large action cross sections, free from fluorescence quenching and tunable emission of efficient non-doped organic light-emitting diodes†

Bingjia Xu,‡[a] Jiajun He,‡[a] Yang Liu,[b] Bin Xu,[b] Qiangzhong Zhu,[c] Mingyuan Xie,[c] Zebo Zheng,[c] Zhenguo Chi,*[a] Wenjing Tian,[b] Chongjun Jin,[c] Fuli Zhao,[c] Yi Zhang[a] and Jiarui Xu*[a]

Received 17th October 2013
Accepted 16th January 2014

DOI: 10.1039/c3tc32052a

www.rsc.org/MaterialsC

Two novel quadrupolar D–π–D type two-photon absorption (2PA) luminophores $PA_2F_4H_8E_8$ and $AnA_2F_4H_8E_8$ were synthesized by Wittig–Horner reaction in high yields. By using distyrylbenzene as the π-bridge center, $PA_2F_4H_8E_8$ shows two-photon absorption aggregation-induced emission enhancement (2PA-AIEE) and exhibits exceptionally large 2PA and 2PA action cross-sections up to ~6300 GM and ~1400 GM at 800 nm in THF, respectively. A non-doped electroluminescent (EL) device of $PA_2F_4H_8E_8$ displays good performance with an extremely low turn-on voltage of 2.6 V and a high brightness of 9837 cd m^{-2}.

Introduction

Organic two-photon absorption (2PA) luminophores have attracted tremendous interest due to their promising applications, such as two-photon fluorescence probes,[1–4] two-photon fluorescence microscopy,[5–7] and three-dimensional (3D) optical data storage.[8–10] These applications utilize a key feature of the molecules, namely, the two-photon excited fluorescence (TPEF), which can provide attractive advantages including increased depth penetration, improved spatiotemporal resolution, reduced photodamage, and high signal-to-noise ratio.[11–13]

For efficient TPEF, a large 2PA action cross-section ($\Phi_F\delta_2$) is often required. The 2PA action cross-section has been associated with the two-photon absorption cross-section (δ_2) and the fluorescence quantum yield (Φ_F) of the luminophore, and is defined as a product of $\delta_2 \times \Phi_F$.[14] To enhance the δ_2 values, extensive research efforts have been made and the studies have focused mostly on π-conjugated organic dyes with different structure motifs, including donor–π-bridge–donor (D–π–D),[15–19] donor–acceptor–donor (D–A–D),[20–22] and donor–π-bridge–acceptor (D–π–A).[23–25] The results of these studies reveal that the magnitude of δ_2 depends on the effective π-conjugated length of the dyes and the degree of intramolecular charge transfer (ICT) upon excitation.[26,27] Based on this guideline, substantial amounts of 2PA materials have been developed and satisfactory δ_2 values have been achieved.[19,28] However, those of 2PA luminophores often are compromised with decreased fluorescence quantum yields when they are dissolved in polar media with high water content, which is extremely important for biological samples, due to the solvent relaxation process.[6,29–31] In addition, the conventional π-conjugated organic luminophores also suffer quenching effects when they are in high concentration or in the solid state because of the strong intermolecular π–π stacking interactions and radiationless decay.[32–34] The latter phenomenon is also notoriously known as aggregation-caused quenching (ACQ).[35–37] To surmount this ACQ effect, some 2PA dyes with aggregation-induced emission (AIE) properties have been reported. Such AIE dyes show high Φ_F values in aggregation states, which is opposite to the conventional 2PA luminophores. Their fluorescence in solution, nevertheless, is extremely weak (Φ_F < 1%) due to the radiationless decay caused by intramolecular rotation.[38–40] These quenching effects lead to low Φ_F values, giving most $\Phi_F\delta_2$ products <1000 GM which could not meet the requirements of practical applications well.[32] Hence, there is an urgent need to develop an approach to

[a]PCFM Lab, DSAPM Lab, KLGHEI of Environment and Energy Chemistry, State Key Laboratory of Optoelectronic Material and Technologies, School of Chemistry and Chemical Engineering, Sun Yet-sen University, Guangzhou 510275, China. E-mail: chizhg@mail.sysu.edu.cn; xjr@mail.sysu.edu.cn; Fax: +86 20 84112222; Tel: +86 20 84112712

[b]State Key Laboratory of Supermolecular Structure and Material, Jilin University, Changchun 130012, China

[c]State Key Laboratory of Optoelectronic Material and Technologies, School of Physics and Engineering, Sun Yat-sen University, Guangzhou 510275, China

† Electronic supplementary information (ESI) available: Scheme S1; Table S1–S3; Fig. S1–S22; structure information of the compounds (NMR, IR, and MS spectra). See DOI: 10.1039/c3tc32052a

‡ Theses authors contributed equally to the preparation of this work.

overcome the fluorescence quenching effects of 2PA luminophores with large two-photon absorption.

Recently, another kind of anti-ACQ compound was found by Tang[41] and Park[42] called aggregation-induced emission enhancement (AIEE) materials. These compounds would be excellent candidates as 2PA luminophores if they afford large δ_2 values, because their molecules may show not only high fluorescence in dilute solution, but more importantly, their unique molecular structures endow them advantages to prevent the formation of detrimental π–π interactions and exhibit significantly higher Φ_F values in concentrated solutions or the solid state.[43–46] Particularly, in polar media with high water content, the AIEE compounds can maintain strong fluorescence by forming nanoparticles.[47,48] Therefore, development of organic luminophores with large effective π-conjugated length and AIEE properties would be an ideal approach to enhance two-photon absorption and overcome the fluorescence quenching simultaneously. On the other hand, as 2PA-AIE has only been found in all-conjugated dyes, it is thus more interesting to investigate whether the AIE moieties remain offering positive contributions to the fluorescence emission enhancement of the desired compounds by non-conjugation attachment.

In this contribution, we are trying to demonstrate such a new strategy. Triphenylamine and fluorene are the most widely used building blocks for the construction of dyes with high two-photon absorptivity, as well as excellent thermal stability.[49–51] Moreover, their derivatives often show hole-transport ability and strong fluorescence in solution.[52,53] We thus employed fluorenyl-substituted triphenylamine as electron donor and distyrylbenzene (DSB)/9,10-distyrylanthracene (DSA) as π-bridge to construct symmetric quadrupolar D–π–D cores, which may lead to large two-photon absorption and strong fluorescent emission in the monomeric form. DSB and DSA are chosen as the centers due to their planar or distorted molecular structures, which can mediate both the π-conjugated length and Φ_F value of the new 2PA luminophores. Meanwhile, tetraphenylethylene (TPE) is used as periphery by non-conjugation attachment to ensure the fluorescence enhancement from solution to solid state because of its unique AIE behavior: it is nonemissive when dissolved in dilute solution but becomes luminescent when aggregated, which is exactly opposite to the ACQ effect.[43] Such judicious structure design has made us succeed in creating a novel type of 2PA luminogen that is free from quenching effects not only in dilute solution, but also in solid thin film and polar media with high water content. Additionally, the strongly fluorescent compound can also act as hole-transporting and light-emitting material for OLED applications with high brightness, which has not been achieved for 2PA luminophores with large δ_2 values so far.

Results and discussion

Synthesis

The desired luminogens were prepared according to the synthetic routes depicted in Scheme 1, whilst the detailed procedures for the synthesis are described in the experimental section. Briefly, FHE_2B was synthesized by introducing bromohexyloxytetraphenylethylene (TPEOH) to 2-bromo-9*H*-fluorene, followed by metathesis of the bromine atom by boron pinacolate. Coupling of 4-(bis(4-iodophenyl)amino)benzaldehyde with FHE_2B was catalyzed by $Pd(PPh_3)_4$ giving $AF_2H_4E_4$ in a good yield of 71%. The desirable compounds $PA_2F_4H_8E_8$ and $AnA_2F_4H_8E_8$ were prepared by Wittig–Horner reaction by introducing $AF_2H_4E_4$ to the corresponding ylide reagents 1,4-bis(diethylphosphorylmethyl)benzene ($Bpho_2$) and 9,10-bisdiethylphosphorylmethyl)anthracene ($Anpho_2$), respectively. Meanwhile, $PA_2F_4H_4$ and $AnA_2F_4H_8$ were also synthesized by using the same methods without tetraphenylethylene as periphery (Scheme S1†). All the intermediates and final products were characterized spectroscopically with satisfactory data obtained which confirmed their expected molecular structures. The dyes are soluble in common organic solvents such as dichloromethane, chloroform, tetrahydrofuran (THF) and *N*,*N*′-dimethylformamide (DMF), but insoluble in water.

Photophysical properties

The UV-visible absorption spectra of $PA_2F_4H_8E_8$ and $AnA_2F_4H_8E_8$ were measured in THF solutions. As shown in Fig. 1 and summarized in Table 1, two intense absorption bands were observed at 314–370 nm for $PA_2F_4H_8E_8$ and 314–360 nm for $AnA_2F_4H_8E_8$, which could be assigned as the absorptions associated with the periphery tetraphenylethylene (314 nm)[54] and the fluorenylphenyl-substituted aminostyryl segment of $PA_2F_4H_8E_8$ (370 nm) and $AnA_2F_4H_8E_8$ (360 nm),[55,56] respectively. The bathochromic shift of the transition band from 360 nm to 370 nm could be attributed to the enhanced electronic coupling between the fluorenyl-substituted triphenylamine component and distyrylbenzene (DSB) in $PA_2F_4H_8E_8$, which resulted in the more extended π-conjugation length on the long axis of the molecule.[57,58] In addition, both $PA_2F_4H_8E_8$ and $AnA_2F_4H_8E_8$ exhibited a broad absorption band at ≥420 nm which might be attributed to the $^1\pi$–π* transition of the core. The emission maxima of the $PA_2F_4H_8E_8$ and $AnA_2F_4H_8E_8$ in THF solutions were located at 480 nm and 561 nm, while those of their corresponding cores and the peripheral hexyloxy-substituted TPE unit (TPEH) were 480, 561, and 435 nm (Fig. S1A†), respectively, indicating that the emissions of $PA_2F_4H_8E_8$ and $AnA_2F_4H_8E_8$ in THF solution mainly originated from their cores. However, in the solid state, $PA_2F_4H_8E_8$ and $AnA_2F_4H_8E_8$ emitted bluish-green and orange light with emission maximum at 482 nm and 586 nm, respectively (Fig. 1), which were both located between the emission of the TPEH unit and the corresponding core (Fig. S1B,† 465 nm for TPEH, 517 nm for $PA_2F_4H_8$, and 608 nm for $AnA_2F_4H_8$). This observation suggested that both the TPE and the central chromophore had contributions to the fluorescence of $PA_2F_4H_8E_8$ and $AnA_2F_4H_8E_8$ in the solid state. The PL peak position of the $PA_2F_4H_8E_8$ thin film was only slightly red-shifted (peak to peak difference is 2 nm) from the spectrum of its dilute solution in THF, whereas the spectral shift from solution to solid thin film of $AnA_2F_4H_8E_8$ was about 25 nm.

In addition, the fluorescence weighted mean lifetimes ($\langle\tau\rangle$) of $PA_2F_4H_8E_8$ and $AnA_2F_4H_8E_8$ in the solid state were estimated to be 1.04 ns and 2.05 ns by fitting the decay curves (Fig. S2 and

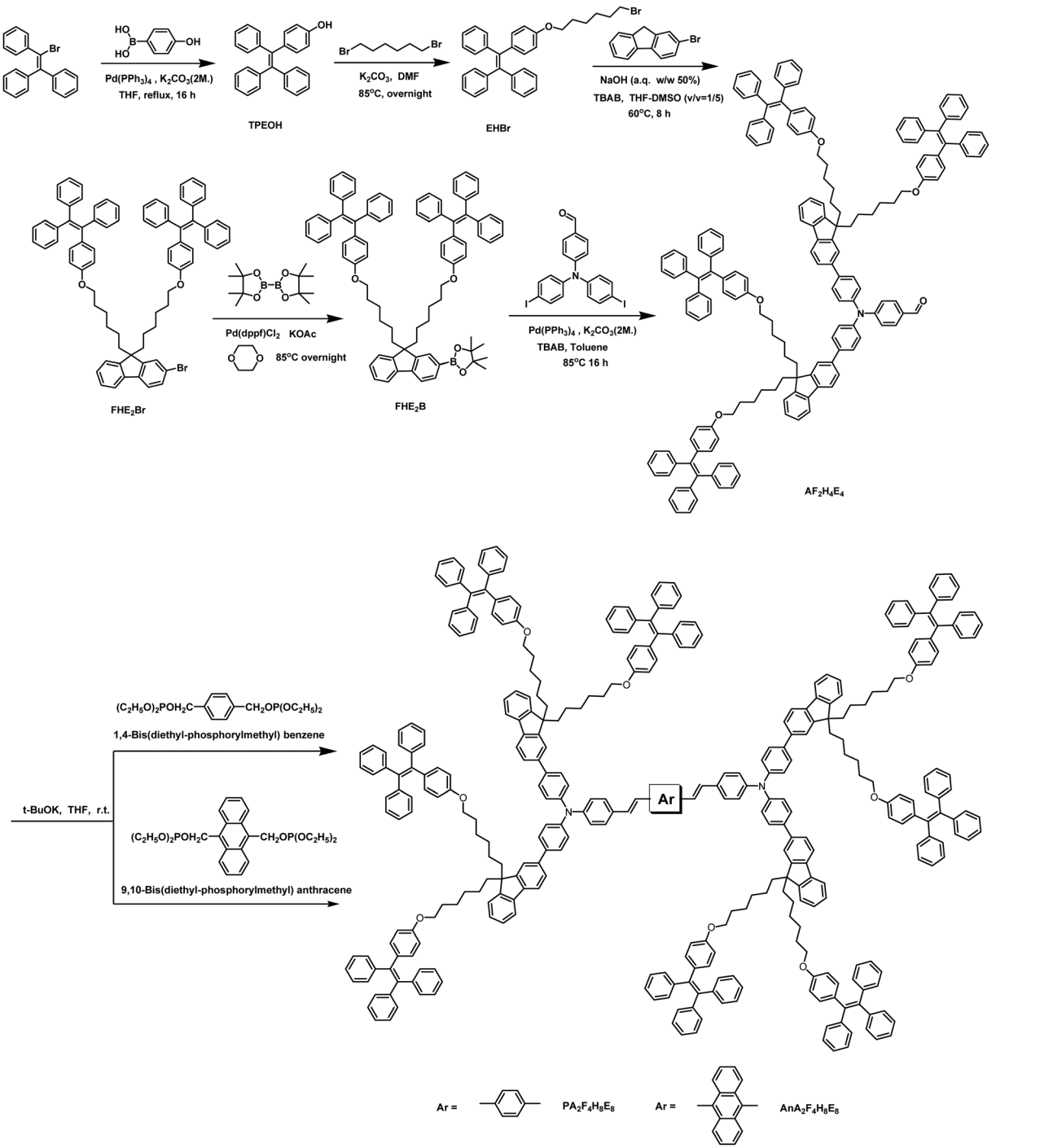

Scheme 1 Synthetic routes to the desired compounds.

Table S1†). The longer lifetime of $AnA_2F_4H_8E_8$ could be attributed to the greater steric hindrance effect caused by the distorted DSA moiety, which led to fewer intramolecular or intermolecular interactions in the solid state.[59] Careful inspection of the decay curves revealed that $PA_2F_4H_8E_8$ and $AnA_2F_4H_8E_8$ had three and four fluorescence relaxation pathways, respectively. For $PA_2F_4H_8E_8$, the excited molecules mainly decayed through the first pathway ($\tau_1 = 0.74$, $A_1 = 60\%$). However, for $AnA_2F_4H_8E_8$, the second pathway ($\tau_2 = 1.72$) was found to be 70%, playing a predominant role. The multi-lifetimes may be ascribed to different conformations of the new luminophores in the excited state by considering the bulky core and periphery groups in the dyes.[60]

Aggregation-induced emission (enhancement)

Solution of $PA_2F_4H_8E_8$ emitted strong fluorescence when illuminated with a UV lamp, whereas solid powder of $PA_2F_4H_8E_8$

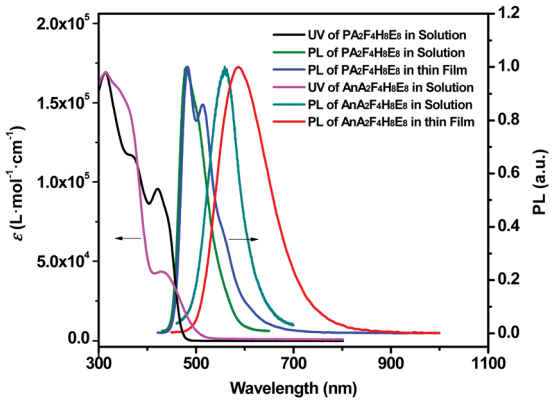

Fig. 1 Photophysical properties of the compounds.

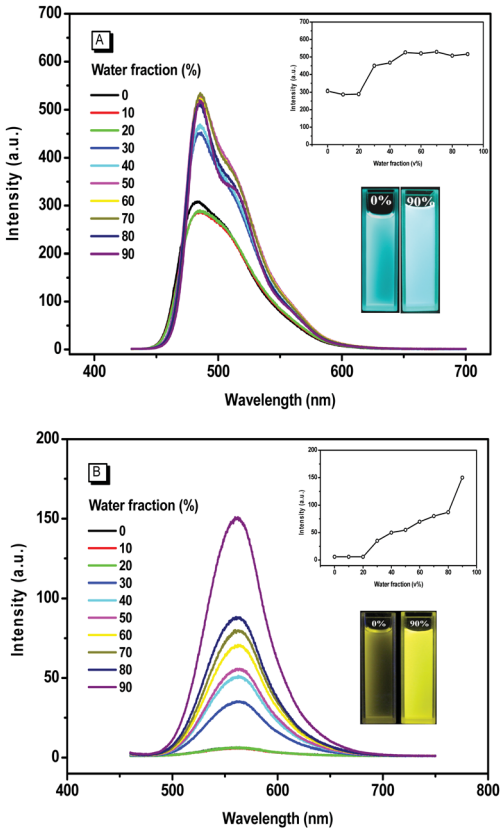

Fig. 2 PL spectra of the dilute solutions of $PA_2F_4H_8E_8$ (A) and $AnA_2F_4H_8E_8$ (B) in water/THF mixtures with different water fractions (concentration: 10 μM). The insets depict changes in PL peak intensity (upper) and emission images of the compounds in pure THF and 90% water fraction mixture under 365 nm UV illumination (10 μM) (lower).

was more emissive (Fig. S15†), thus indicating that aggregated formation resulted in fluorescence emission enhancement. To verify this observation, distilled water was added to the THF solution of $PA_2F_4H_8E_8$, and then the PL spectrum was investigated. Since water is a poor solvent for this hydrophobic luminophore, its molecules must aggregate in solvent mixtures with high water content. As depicted in Fig. 2A, strong PL signal was recorded for $PA_2F_4H_8E_8$ in pure THF with a peak intensity of 307 a.u. However, with an increase in water fraction (f_w) up to 20%, the emission intensity decreased to 289 a.u. and a red shift of 5 nm in peak position was also observed, which should be attributed to the solvent relaxation process caused by the dipole–dipole interaction between the fluorescent molecule in its excited state and the surrounding solvent molecules. On the other hand, with f_w higher than 20%, the emission was recovered and started to rise with an increase in intensity of up to about 1.8 times in 90% aqueous mixture. This remarkable enhancement is further supported by the image shown in Fig. 2A. Although the aqueous mixtures were macroscopically homogeneous, the Mie scattering effect[61] observed in UV-visible absorption spectra of $PA_2F_4H_8E_8$ (Fig. S4A†) revealed that nanoaggregates of the luminophore were formed in the mixtures with f_w > 20%. Evidently, the fluorescence enhancement of the luminophore was induced by aggregation formation. In other words, $PA_2F_4H_8E_8$ is AIEE-active. In contrast, compound $AnA_2F_4H_8E_8$ emitted extremely weak fluorescence in solution as compared to $PA_2F_4H_8E_8$. Its aggregates, however, became emissive (Fig. 2B and Fig. S4B†). The PL peak intensity of $AnA_2F_4H_8E_8$ continuously increased with increasing water content in the water/THF mixtures and reached a maximum at an f_w value of 90%. $AnA_2F_4H_8E_8$ is thus an AIE emitter.

The AIEE/AIE activity of the compounds can be further validated by the comparison of Φ_F values in solution and aggregation states. While the Φ_F values of $PA_2F_4H_8E_8$ and $AnA_2F_4H_8E_8$ in THF solution were 22% and 0.8%, those of their nanoaggregates in 90% aqueous mixtures were boosted to 35% and 8.8%, respectively (Table 1 and Fig. S5†). Further enhancement was observed for their solid thin films with Φ_F values up to 37% and 66%, resulting in AIEE/AIE factors ($\alpha = \Phi_{F,\ thin\ flim}/\Phi_{F,\ 0\%}$) as high as 1.8 and 81, respectively, thus testifying their AIEE/AIE natures.

Table 1 Optical properties of the compounds

Compound	λ_{abs}[a] (nm)	λ_{em} (nm)		$\Phi_{F,0\%}$[d]	$\Phi_{F,90\%}$[e]	$\Phi_{F,\ thin\ film}$[f]	α[g]	δ_2[h] (GM)	$\Phi_F\delta_2$[i] (GM)
$PA_2F_4H_8E_8$	314; 370; 420	480[b]	482; 514[c]	0.21	0.35	0.37	1.8	6300	1400
$AnA_2F_4H_8E_8$	314; 360; 428	561[b]	586[c]	0.0081	0.088	0.66	81	5100	40

[a] UV-visible absorption band in THF. [b] One-photon excited PL wavelength in THF. [c] One-photon excited PL wavelength of solid thin film. [d] Fluorescence quantum yield in THF, using fluorescein in 0.1 N NaOH as standard. [e] Fluorescence quantum yield in mixtures of water/THF = 9 : 1 (v/v), using fluorescein in 0.1 N NaOH as standard. [f] Fluorescence quantum yield in solid thin film. [g] $\alpha = \Phi_{F,\ solid}/\Phi_{F,\ 0\%}$. [h] Two-photon absorption cross-section in THF. [i] Two-photon absorption action cross-section in THF.

It is noticeable that $PA_2F_4H_8E_8$ and $AnA_2F_4H_8E_8$ exhibited different fluorescent behaviours in *n*-hexane/CH_2Cl_2 mixtures as compared to the water/THF system. As shown in Fig. S6 and Fig. S7,† with the increase of *n*-hexane fraction in the range of 0% to 80%, the absorption profiles of $PA_2F_4H_8E_8$ and $AnA_2F_4H_8E_8$ were almost unchanged and no Mie scattering effect was observed, indicating that the solvating power of the solvent mixture was still high enough to dissolve the fluorescent molecules. In contrast, the emission of $PA_2F_4H_8E_8$ was enhanced continuously accompanied by a spectral shift to the shorter wavelength region due to the polarity decrease of the mixture. On the other hand, no obvious change was found for the emission of $AnA_2F_4H_8E_8$ in *n*-hexane/CH_2Cl_2 mixture with *n*-hexane fraction ≤80%, which might be ascribed to its smaller dipolar moment change and weak signal response caused by the radiationless decay of the compound. Further increase of the *n*-hexane content resulted in unstable mixtures, leading to formation of precipitates of $PA_2F_4H_8E_8$ and $AnA_2F_4H_8E_8$.

To acquire more insight the origin of the AIEE/AIE properties of $PA_2F_4H_8E_8$ and $AnA_2F_4H_8E_8$, distilled water was added to the THF solutions of the cores ($PA_2F_4H_8$ and $AnA_2F_4H_8$), and the UV and PL results are depicted in Fig. S3 and Fig. S4.† Intriguingly, with the increase of water content, $PA_2F_4H_8$ and $AnA_2F_4H_8$ also showed notable AIEE and AIE effects, respectively, revealing that the attractive AIEE/AIE properties of $PA_2F_4H_8E_8$ and $AnA_2F_4H_8E_8$ might originate from both the peripheral TPE group and the cores of these two compounds. Noticeably, although $PA_2F_4H_8$ and $AnA_2F_4H_8$ were AIEE/AIE-active, both of their fluorescent quantum yields in solid state (16% for $PA_2F_4H_8$ and 30% for $AnA_2F_4H_8$) were much lower than their corresponding matrixes $PA_2F_4H_8E_8$ and $AnA_2F_4H_8E_8$. Decoration with peripheral TPE groups through non-conjugation attachment thus made a great contribution towards the fluorescence emission and changed their molecules to be more emissive in the solid state, which is of importance for the fabrication of high efficiency solid emitters.

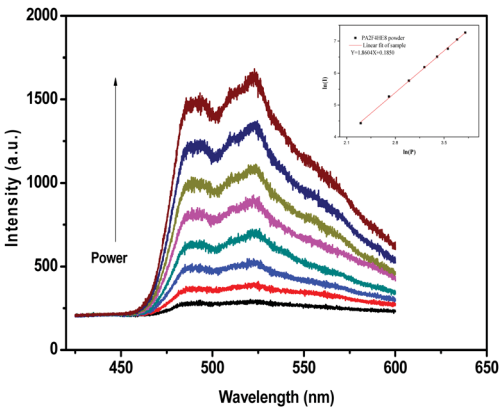

Fig. 3 Two-photon fluorescence (TPF) emission spectra of $PA_2F_4H_8E_8$ in the solid state with different input powers; the inset depicts the plot of the emission intensity *versus* input laser power for $PA_2F_4H_8E_8$ on a log/log scale. The fit of the experimental data is shown in black, and the corresponding equation is reported in the inset. The excitation source was an 800 nm femtosecond laser.

Two-photon absorption and two-photon excited fluorescence

The δ_2 values of these luminophores were measured by open-aperture Z-scan technique,[62,63] in which a femtosecond (125 fs, 800 nm) Ti–sapphire laser was used for the measurement to eliminate the effect of one-photon absorption. As shown in Fig. 3 and Fig. S8,† the up-conversion fluorescence signals of $PA_2F_4H_8E_8$ and $AnA_2F_4H_8E_8$ show quadratic dependence on the intensity of the excitation laser beam. The experimental regression coefficients of $PA_2F_4H_8E_8$ and $AnA_2F_4H_8E_8$ were estimated to be 1.86 and 2.06, respectively, indicating that no photodegradation or saturation occurred in the experimental laser power, firmly supporting that the fluorescence arose from two-photon absorption process.[64]

The typical Z-scan curves and fitting curves of $PA_2F_4H_8E_8$ and $AnA_2F_4H_8E_8$ are displayed in Fig. S9 and Fig. S10,† while the corresponding δ_2 values are listed in Table 1. At 800 nm, a wavelength that is practically useful for biophotonic applications, $PA_2F_4H_8E_8$ and $AnA_2F_4H_8E_8$ exhibit exceptionally large 2PA cross sections of ~6300 GM and ~5100 GM, respectively, which are larger than most of the representative materials.[19,65,66] It is worth noting that the δ_2 values of $PA_2F_4H_8E_8$ and $AnA_2F_4H_8E_8$ are also much higher than those 2PA dyes with the same π-bridges DSB and DSA.[17,67–69] It is thus believed that such impressively high δ_2 values should be ascribed to their efficient electron donor, that is, the fluorenyl-substituted triphenylamine, and their symmetric D–π–D structure motif. Moreover, as compared to $AnA_2F_4H_8E_8$, $PA_2F_4H_8E_8$ showed even higher 2PA absorption. According to the previous studies, the quadrupolar framework for the core of $AnA_2F_4H_8E_8$ is likely to be distorted severely due to the large internal steric hindrance between the anthrylene center and vinylene moieties.[67,68] It is concluded that the more rigid and planar geometry for the core of $PA_2F_4H_8E_8$ in the monomeric form may play a crucial role in extending the effective conjugation on the long axis of the molecule, and then, leading to the increase of 2PA cross-section.[70]

To further verify the reason for the enhancement of δ_2 value, linear absorption and emission spectra for these two compounds in common solvents were also measured (Fig. S12 and Fig. S13†), and their photophysical properties are listed in Table S2.† The absorption of tetraphenylethylene was hypochromic-shifted as the polarity of the solvent was increased, suggesting less conjugation and greater distortion of the periphery tetraphenylethylene. Noticeably, the absorption profiles and maxima for the cores at 360–428 nm of both compounds were almost identical in various solvents, indicating that their ground state electronic structures had small dipole moments and were solvent polarity independent. However, the fluorescence spectra were more strongly affected by the solvent polarity. The fluorescence peaks of $PA_2F_4H_8E_8$ and $AnA_2F_4H_8E_8$ showed a red shift of about 37 nm and 18 nm in solvents going from nonpolar toluene to highly polar DMF, exhibiting an obvious solvatochromic effect. The Stokes shifts

($\Delta\nu$) of $PA_2F_4H_8E_8$ and $AnA_2F_4H_8E_8$ in varying solvents were calculated and their solvatochromic behaviors could be described by the Lippert–Mataga equation:[48]

$$\Delta\nu = \nu_a - \nu_e = \frac{2\Delta f}{hca^3}(\mu_e - \mu_g)^2 + \text{constant} \quad (1)$$

where ν_a and ν_e represent the maximum absorbance and emission wavenumber; μ_e and μ_g are the dipole moments (1 D = 10^{-18} esu cm) of excited and ground states, respectively; h is the Planck constant 6.63 × 10^{-27} (erg s), c is the speed of light 3 × 10^{10} (cm s^{-1}), and a is the Onsager solvent cavity radius.

Δf is defined as orientational polarizability and chosen as the measure of polarity:

$$\Delta f = \frac{\varepsilon - 1}{2\varepsilon + 1} - \frac{n^2 - 1}{2n^2 + 1} \quad (2)$$

where ε is the static dielectric constant and n is the optical refractive index of the solvent.

The large slopes of $\Delta\nu$ *vs.* Δf depicted in Fig. S11 suggest that the excited states of $PA_2F_4H_8E_8$ and $AnA_2F_4H_8E_8$ have larger dipolar moments than the ground states because of the substantial charge redistribution,† in which a non-equilibrated excited state species is created upon Franck–Condon excitation, followed by the solvent relaxation to the equilibrated state.[71]

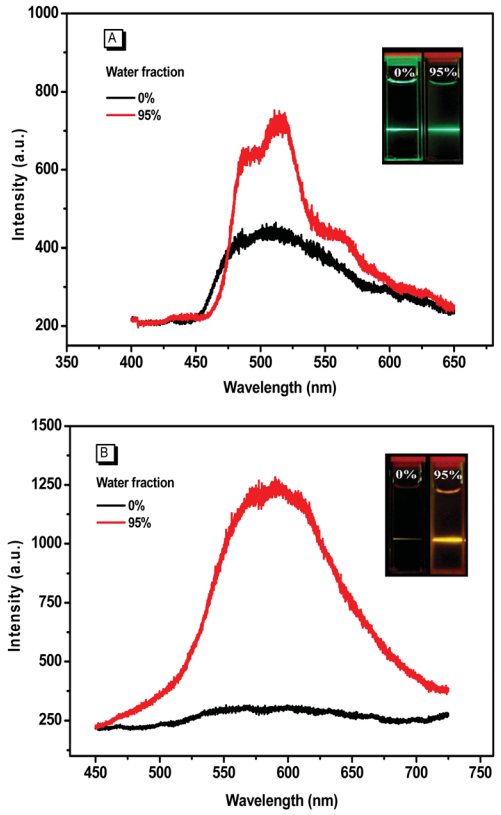

Fig. 4 Two-photon fluorescence (TPF) emission spectra of the dilute solutions of $PA_2F_4H_8E_8$ (A) and $AnA_2F_4H_8E_8$ (B) in water/THF mixtures with different water fractions (concentration: 10 μM; excitation: 800 nm femtosecond laser). The insets depict TPF emission images of the compounds in pure THF and 95% water fraction mixture under 800 nm femtosecond laser illumination (10 μM).

The steeper slope obtained with $PA_2F_4H_8E_8$ indicates that $PA_2F_4H_8E_8$ undergoes a larger dipolar moment change ($\mu_e - \mu_g$) than that of $AnA_2F_4H_8E_8$.[72] On considering that the only difference in molecular structure is the π-bridge center, it is believed that the larger change in dipolar moment of $PA_2F_4H_8E_8$ is probably attributed to its longer effective π-conjugation caused by the higher coplanarity, which finally leads to the increase of 2PA cross-section.[26]

Combining these results with the determination of Φ_F values in THF solutions provides for $\Phi_F\delta_2$ values of ~1400 GM and ~40 GM for $PA_2F_4H_8E_8$ and $AnA_2F_4H_8E_8$, respectively. Except for very few squaraine[73] and cyanostyrene[32] derivatives, the $\Phi_F\delta_2$ value of $PA_2F_4H_8E_8$ is among the highest reported at 800 nm excitation for organic 2PA luminophores. As depicted in Fig. 4A, strong TPEF with peak intensity of 440 a.u. was observed for $PA_2F_4H_8E_8$ because of its large 2PA action cross-section, which met the requirement of practical applications well, even in solution state. Further enhancement was achieved for its nanoaggregates in a 90% aqueous mixture with TPEF peak intensity of 730 a.u., about 1.7 times higher than that in pure THF. The significant enhancement in emission indicates that $PA_2F_4H_8E_8$ is two-photon excited AIEE active. As most of the 2PA luminophores suffer TPEF quenching effects when dissolved or dispersed in polar media with high water content, such unique two-photon excited AIEE properties, as well as the large 2PA action cross section, endow $PA_2F_4H_8E_8$ with attractive advantages in biophotonic applications, such as two photon microscopy (TPM).[74,75] On the other hand, $AnA_2F_4H_8E_8$ showed two-photon excited AIE property because it exhibited weak TPEF in solution with low $\Phi_F\delta_2$ value but became highly emissive in 90% aqueous mixture (Fig. 4B). Moreover, both $PA_2F_4H_8E_8$ and $AnA_2F_4H_8E_8$ emitted strong TPEF in the solid state with wavelengths at 490 and 521 nm for $PA_2F_4H_8E_8$ and 589 nm for $AnA_2F_4H_8E_8$, which were close to the corresponding one-photon solid thin film (Fig. S14 and Fig. S15†).

Thermal, morphological and electrochemical properties

Both $PA_2F_4H_8E_8$ and $AnA_2F_4H_8E_8$ are thermally stable. As shown in Fig. S16 and Table S3,† the decomposition temperatures of $PA_2F_4H_8E_8$ and $AnA_2F_4H_8E_8$ with 5% weight loss under N_2 atmosphere (T_d) are as high as 423 °C and 438 °C, respectively. The T_d of $AnA_2F_4H_8E_8$ is slightly higher than that of $PA_2F_4H_8E_8$, probably due to the higher planarity and rigidity of the anthracene unit. The glass transition temperatures (T_g) were detected at 118 °C for both $PA_2F_4H_8E_8$ and $AnA_2F_4H_8E_8$ (Fig. S17†), revealing that they also enjoyed high morphological stability. Additionally, no melting points were observed for both $PA_2F_4H_8E_8$ and $AnA_2F_4H_8E_8$ in the first and second heating runs, implying that the pristine compounds were amorphous and had extremely low tendency to crystallize. Moreover, the powder X-ray diffraction (XRD) patterns of $PA_2F_4H_8E_8$ and $AnA_2F_4H_8E_8$ displayed relatively broad and random scattering peaks (Fig. S18†), clearly demonstrating the non-crystalline amorphous nature of $PA_2F_4H_8E_8$ and $AnA_2F_4H_8E_8$ in the solid state, which was in good agreement with the DSC results. Such amorphous dyes with high T_g values

could have a better chance for retaining the film morphology during device operation.

To investigate the electrochemical properties of the new luminophores with peripheral tetraphenylethylene groups, cyclic voltammetry (CV) measurements were performed with the ferrocene/ferrocenium (Fc/Fc^+) redox couple as external standard. Fig. S19 shows CV curves of the compounds and the details of their electrochemical properties are listed in Table S3.† During anodic scans between 0 and 2.0 V in CH_2Cl_2, two oxidation peaks were observed at 1.35 and 1.54 V for $PA_2F_4H_8E_8$ and at 1.35 and 1.51 V for $AnA_2F_4H_8E_8$. The highest occupied molecular orbital (HOMO) energy levels of $PA_2F_4H_8E_8$ and $AnA_2F_4H_8E_8$ estimated from oxidation-onset potentials (1.17 V for $PA_2F_4H_8E_8$ and $AnA_2F_4H_8E_8$) were both −5.44 eV, while the lowest occupied molecular orbital (LUMO) energy levels were calculated to be −2.79 and −2.95 eV, respectively. The HOMO energy levels approached the work function of ITO/poly(-styrenesulfonate)-doped poly(3,4-ethylenedioxythiophene) (PEDOT : PSS, −5.2 eV), which thereby facilitate the transfer of holes. Additionally, $PA_2F_4H_8E_8$ showed a higher LUMO value than $AnA_2F_4H_8E_8$. The higher LUMO energy level of $PA_2F_4H_8E_8$ is beneficial for obstructing electrons to overflow the emissive layer and encounter the anode, which may lead to more efficient exciton recombination.[76]

Electroluminescence device properties

Excellent thermal stabilities, good morphological stabilities, suitable HOMO energy levels, and high Φ_F values in solid thin films are achieved at the same time for the new 2PA luminophores, as mentioned above, and thus good performance of non-doped electroluminescence (EL) devices is expected. Since triphenylamine is well known as a hole-transporting material,[77] the luminophores of $PA_2F_4H_8E_8$ and $AnA_2F_4H_8E_8$ derived from triphenylamine may have the ability to act as hole-transporting and light-emitting materials simultaneously. With these in mind, we fabricated two organic light-emitting diodes (OLEDs, devices I and II) by using a spin-coating process with the device configuration of ITO/PEDOT : PSS (30 nm)/HTL-LEL (40 nm)/Alq_3 (40 nm)/LiF(1 nm)/Al (100 nm), where PEDOT : PSS is poly(3,4-ethylenedioxythiophene) : poly(styrene sulfonic acid) (hole injection layer); Alq_3 is tris(8-hydroxyquinolinato) aluminium (electron-transport layer); the HTL (hole-transport layer) and LEL (light-emitting layer) is $PA_2F_4H_8E_8$ or $AnA_2F_4H_8E_8$, and ITO is indium tin oxide (anode). Fig. 6 and Table 2 summarize the EL characteristics of the devices.

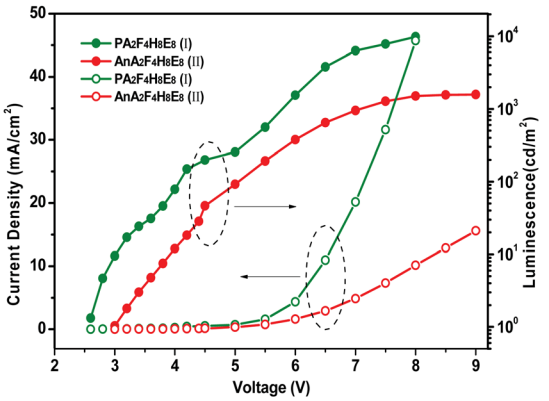

Fig. 6 Current density–voltage–luminance characteristics.

Table 2 Device properties of the compounds

Device	EL_{max}[a] (nm)	V_{on}[b] (V)	L_{max}[c] (cd m^{-2})	$\eta_{p,max}$[d] (lm W^{-1})	$\eta_{c,max}$[e] (cd A^{-1})
$PA_2F_4H_8E_8$ (I)	516	2.6	9837	1.07	1.10
$AnA_2F_4H_8E_8$ (II)	570	3.0	1577	0.60	0.86
$PA_2F_4H_8E_8$ (III)	480	3.0	5625	1.93	1.71
$AnA_2F_4H_8E_8$ (IV)	542	6.2	1424	0.84	1.67

[a] Maximum of EL wavelength, measured at 8 V. [b] Turn on voltage, recorded at 1 cd m^{-2}. [c] Maximum luminance. [d] Maximum power efficiency. [e] Maximum current efficiency. EL device: ITO/PEDOT : PSS (30 nm)/X/LiF (1 nm)/Al (100 nm); for device (I): $PA_2F_4H_8E_8$ (40 nm)-Alq_3 (40 nm); for device (II): $AnA_2F_4H_8E_8$ (40 nm)-Alq_3 (40 nm); for device (III): $PA_2F_4H_8E_8$ (40 nm)–TPBi (50 nm); for device (IV): $AnA_2F_4H_8E_8$ (35 nm)–TPBi (40 nm).

Using Alq_3 as an electron transport layer, the device of $AnA_2F_4H_8E_8$ (device II) exhibited a low turn-on voltage (V_{on}) at 3.0 V, with the maximum luminescence (L_{max}) and power efficiency ($\eta_{p,max}$) being 1577 cd m^{-2} and 0.60 lm W^{-1} at 9 V, respectively, showing a moderate device performance. However, when the HTL-LEL was changed to be $PA_2F_4H_8E_8$ (device I), the device was turned on by an extremely low voltage (2.6 V) and emitted much more intensely (L_{max} = 9837 cd m^{-2}) and efficiently (1.07 lm W^{-1}) at 8 V, and its brightness was an order of magnitude higher than that of a 2PA-AIE luminophore reported previously (858 cd m^{-2}).[75] To the best of our knowledge, such

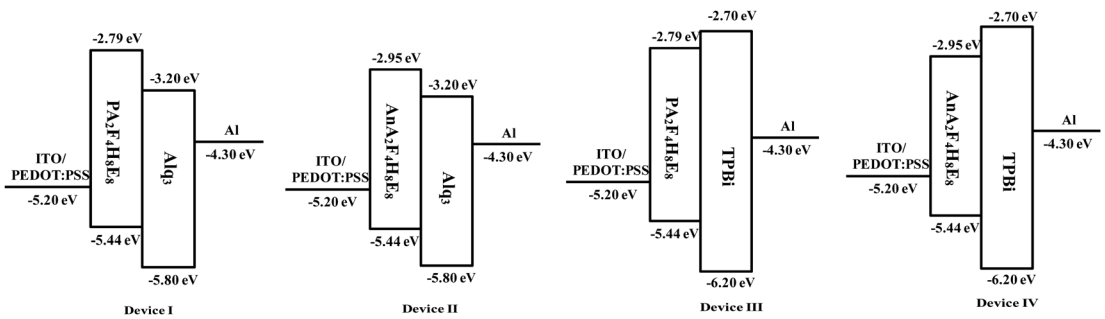

Fig. 5 The energy level diagrams of the devices.

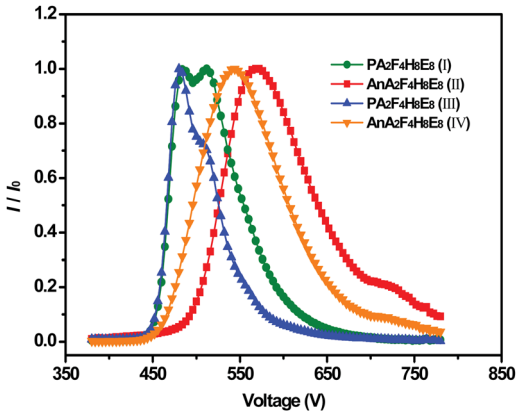

Fig. 7 EL spectra of the compounds.

high device brightness has not been achieved for a 2PA luminophore with large δ_2 value so far. According to the energy level diagrams in Fig. 5, the improved device performance of $PA_2F_4H_8E_8$ should be attributed to the better electron-blocking capability of $PA_2F_4H_8E_8$ relative to that of $AnA_2F_4H_8E_8$. As a result, more excitons can be confined within the emissive and hole-transport layer.[78] The data attests that the new 2PA-AIEE compound is an excellent hole-transport material with strong fluorescence not only in solution, but also in the solid state. The devices of $PA_2F_4H_8E_8$ and $AnA_2F_4H_8E_8$ emitted a green and greenish yellow light with $CIE_{x,y}$ coordinates of (0.23, 0.48) and (0.46, 0.50), respectively. The peaks of their electroluminescence were estimated to be 484 nm and 511 nm for $PA_2F_4H_8E_8$ and 570 nm for $AnA_2F_4H_8E_8$ (Fig. 7), which might originate from both of the peripheral TPE unit and the cores of the compounds.

Devices III and IV were also fabricated by using $PA_2F_4H_8E_8$ and $AnA_2F_4H_8E_8$ as emitters, respectively, in which the electron transport layer Alq_3 was replaced by 1,3,5-tris(*N*-phenylbenzimidazol-2-yl)benzene (TPBi). Interestingly, device III and device IV displayed bluish green and yellow green light with $CIE_{x,y}$ coordinates of (0.17, 0.40) and (0.38, 0.54) respectively. The peaks of their electroluminescence were 480 nm for $PA_2F_4H_8E_8$ and 542 nm for $AnA_2F_4H_8E_8$, which were both blue-shifted remarkably as compared to devices I and II (Fig. 7). Evidently, the EL emissions of $PA_2F_4H_8E_8$ and $AnA_2F_4H_8E_8$ can be tuned easily between two colors by simply adjusting the device configuration. Additionally, the electroluminescence of device III and device IV was slightly decreased in comparison with the corresponding device with Alq_3 as ETL. As indicated in Fig. 5, the blue shift and the decrease of electroluminescence might be attributed to the imbalance of charge carrier injection caused by the higher LUMO energy level of TPBi. Although the $PA_2F_4H_8E_8$ reported here showed much higher device brightness than most 2PA dyes, its EL device performance remained to be improved as compared to the one-photon absorption luminophores. Further optimization of the OLED devices made with $PA_2F_4H_8E_8$ and $AnA_2F_4H_8E_8$ will be focused on the electron transport layer with different materials and thicknesses.

Conclusions

In summary, we have developed a new strategy to surmount the quenching effects of 2PA luminophores. For our approach, symmetric quadrupolar D–π–D cores with fluorenyl-substituted triphenylamine as electron donor and distyrylbenzene (DSB)/9,10-distyrylanthracene (DSA) as π-bridge were employed to achieve large two-photon absorption and strong fluorescence in solution. Meanwhile, periphery tetraphenylethylene substituents were used by non-conjugation attachment to ensure fluorescence enhancement from solution to aggregation state. Different from the conventional 2PA dyes, which often suffer quenching effects in polar media with high water content or in the solid state, and the typical AIE compounds, whose fluorescences are weak in solution, the novel 2PA-AIEE luminogen $PA_2F_4H_8E_8$ exhibits large $\Phi_F\delta_2$ value and enhanced TPEF from solution to aggregation state, combining the advantages of 2PA and AIE compounds. The unusual AIEE nature and hole-transport capability of the new 2PA luminogen also enable the fabrication of EL devices with good performance and simple structures, further manifesting the success of our approach. To utilize the advantage of high δ_2 and $\Phi_F\delta_2$ values, $PA_2F_4H_8E_8$ is currently being used for cell imaging through two-photon microscopy and the results will be presented in the future.

Experimental

General information

1-Bromo-1,2,2-triphenylethene, 4-hydroxyphenylboronic acid, 1,6-dibromohexane, 2-bromo-9*H*-fluorene, bis(pinacolato) diboron, tetrakis(triphenylphosphine)palladium(0), trimethylborate, and tetrabutyl ammonium bromide (TBAB) were purchased from Alfa Aesar and used as received. All other reagents and solvents were purchased as analytical grade from Guangzhou Dongzheng Company (China) and used without further purification. 4-(Bis(4-iodophenyl)amino)benzaldehyde,[49] 1,4-bis(diethylphosphorylmethyl)benzene,[79] 9,10-bis(diethylphosphorylmethyl)anthracene,[66] and 2-(9,9-dihexyl-9*H*-fluoren-2-yl)-4,4,5,5-tetramethyl-1,3,2-dioxaborolane (FHB)[80] were synthesized according to the literature methods. Tetrahydrofuran (THF) was distilled from sodium/benzophenone. Ultra-pure water was used in the experiments.

Proton and carbon-13 nuclear magnetic resonance spectra (^{1}H NMR and ^{13}C NMR) were measured on a Mercury-Plus 300 spectrometer ($CDCl_3$ as solvents, and tetramethylsilane TMS as the internal standard). Mass spectra (MS) were measured on a Thermo DSQ and LCQ DECA XP and a Bruker Biflex III MS spectrometer. FT-IR spectra were obtained on a Nicolet NEXUS 670 spectrometer (KBr pellet). UV-visible absorption spectra (UV) were determined on a Hitachi U-3900 spectrophotometer. Fluorescence spectra (PL) were measured on a Shimadzu RF-5301PC spectrometer. Thermal behaviors were determined by differential scanning calorimetry (DSC) at heating and cooling rates of 10 °C min^{-1} under N_2 atmosphere using a NETZSCH thermal analyzer (DSC 204F1). Thermogravimetric analyses (TGA) were performed with a thermal analyzer (TA thermal analyzer, Q50) under N_2 atmosphere with a heating rate of 20 °C

min^{-1}. Time-resolved emission decay behaviors were measured on an Edinburgh Instruments Ltd spectrometer (FLSP920). Wide-angle X-ray diffraction (WAXD) measurements were performed by using a Bruker X-ray diffractometer (D8 ADVANCE, Germany) with an X-ray source of Cu Kα ($\lambda = 0.15406$ nm) at 40 kV and 40 mA, at a scan rate of 4° (2θ) min^{-1}.

Cyclic voltammetry (CV) measurement was carried out on a Shanghai Chenhua electrochemical workstation CHI660C in a three-electrode cell with a glassy carbon disk counter electrode, a Ag/AgCl reference electrode, and a Pt working electrode. All CV measurements were performed under an inert argon atmosphere with supporting electrolyte of 0.1 M tetrabutyl ammonium perchlorate (n-Bu_4NClO_4) in dichloromethane at a scan rate of 100 mV s^{-1} using ferrocene as standard. The energy gaps ΔE_g for the compounds were estimated from the absorption edges of UV-visible absorption spectra.

Investigation of two-photon absorption

The two-photon absorption experiments were demonstrated with a regenerative Ti:sapphire amplifier system (spectra Physics Hurricane) with a central wavelength of 800 nm, pulse duration of 125 fs and repetition rate of 1 kHz. The transmitted light was focused into a synchroscan streak camera (Hamamatsu Model C1587) connected to a spectroscope.

The 2PA cross sections (δ_2) of the compounds were measured by the femtosecond open-aperture Z-scan technique according to a previously described method.[62,63] The 2PA coefficient (β) was obtained by data fitting, and the related equation is given as follows:

$$T(z,\ S=1) = \sum_{m=0}^{\infty} \frac{\left[\beta I_0(t) L_{\text{eff}} / \left(1 + z^2/{z_0}^2\right)\right]^m}{(m+1)^{3/2}}$$

where z is the distance between the sample and the focus; $z_0 = k{w_0}^2/2$ is the diffraction length of the beam; $k = 2\pi/\lambda$ is the wave vector; λ is the laser wavelength; $L_{\text{eff}} = (1 - e^{-\alpha L})/\alpha$, where L is the sample length and α is the linear absorption coefficient; $I_0(t)$ is the laser beam irradiance within the sample; $S = 1 - \exp(-2{r_a}^2/{w_a}^2)$ is the aperture linear transmittance, with w_a denoting the beam radius at the aperture in the linear regime and β is the nonlinear absorption coefficient.[81] The 2PA cross section can be calculated using the equation $\sigma = h\nu\beta/N_A C$, in which N_A represents the Avogadro constant and C is the molar concentration of the solute.

Fabrication and characterization of OLEDs

For device fabrication, indium-tin-oxide (ITO)-coated glass with a sheet resistance of 20 Ω cm^{-2} was used as substrate. The ITO glass was routinely cleaned in a ultrasonic cleaning bath with detergent solution, rinsed with acetone, boiled in isopropyl alcohol, rinsed with methanol, and then with de-ionized water in sequence. The PEDOT : PSS was spin-coated on the pre-cleaned ITO glass substrates and then the PEDOT : PSS layer (30 nm) was dried in a vacuum oven at 80 °C for 20 min. The active layers were spin-coated at a speed of 1500 rpm on the top of the PEDOT : PSS layer. The electron-transporting layer Alq_3/TPBi was deposited by thermo-evaporation. The OLEDs were completed by vapour depositing LiF (1 nm) and Al (100 nm) as the cathode through a mask. The EL spectra, luminance CIE coordinates and the current–voltage–luminance characteristics of the devices were measured with a rapid scan system by using a Photo Research PR650 spectrophotometer and a computer-controlled, programmable, direct-current (DC) source. All measurements were carried out at room temperature under ambient atmosphere.

Synthesis of intermediates and final products

TPEOH. To a stirring solution of 1-bromo-1′,2,2′-triphenylethene (8.00 g, 23.9 mmol) in 50 mL of degassed tetrahydrofuran, 4-hydroxyphenylboronic acid (3.95 g, 28.6 mmol), aqueous solution of potassium carbonate (2 M, 14.5 mL, degassed), tetrabutyl ammonium bromide (300 mg), and $Pd(PPh_3)_4$ (50 mg) were added sequentially. Then the reaction mixture was gradually heated to reflux and stirred for 16 h. After workup, the reaction mixture was cooled to room temperature and filtered. Following evaporation of solvent under vacuum, the resulting crude product was purified by column chromatography on silica gel using acetone/n-hexane (v/v = 1/3) as eluent. TPEOH was obtained as a pale yellow powder in 98% yield (8.16 g). ^{1}H NMR (300 MHz, $CDCl_3$) δ (ppm): 7.10–6.93 (m, 15H); 6.87–6.81 (d, 2H); 6.59–6.48 (d, 2H); 4.67–4.55 (s, 1H). ^{13}C NMR (75 MHz, $CDCl_3$) δ (ppm): 153.68, 143.69, 143.59, 140.13, 139.89, 136.07, 132.45, 131.07, 127.43, 127.34, 126.11, 126.00, 114.34; FT-IR (KBr) ν (cm^{-1}): 3520, 3053, 3022, 1600, 1500, 1260, 828, 747, 700; EI-MS, m/z: $[M]^+$ 348, calcd for $C_{26}H_{20}O$ 348; anal. calc. for $C_{26}H_{20}O$: C 89.62, H 5.79, O 4.59; found: C 89.59, H 5.82.

TPEH. To 10 mL of anhydrous N,N-dimethylformamide solution containing 1,6-dibromohexane (1.04 g, 6.31 mmol) and TPEOH (2.00 g, 5.7 mmol), potassium carbonate powder (1.58 g, 11.5 mmol) was added at room temperature. Then the reaction mixture was gradually heated to 85 °C. After stirring overnight, the mixture was cooled, poured into excess ice-cold water, and extracted with dichloromethane three times. The dichloromethane solution was washed with water and dried over $MgSO_4$. Following filtration, the solvent was evaporated under vacuum. The resulting crude product was purified by column chromatography on silica gel using n-hexane as eluent. TPEH was obtained as a white powder in 88% yield (2.17 g). ^{1}H NMR (300 MHz, $CDCl_3$) δ (ppm): 7.21–6.92 (m, 15H); 6.92–6.86 (d, 2H); 6.66–6.57 (d, 2H); 3.96–3.76 (t, 2H); 1.81–1.56 (m, 2H); 1.53–1.27 (m, 6H); 0.95–0.79 (t, 3H). ^{13}C NMR (75 MHz, $CDCl_3$) δ (ppm): 157.76, 144.14, 144.09, 140.02, 1435.92, 131.39, 127.63, 126.38, 126.25, 113.64, 67.86, 31.67, 29.33, 25.80, 22.65, 14.10; FT-IR (KBr) ν (cm^{-1}): 3051, 2930, 2857, 1603, 1506, 1442, 1242, 699; EI-MS, m/z: $[M]^+$ 432, calcd for $C_{32}H_{32}O$ 432.

EHBr. To 15 mL of anhydrous N,N-dimethylformamide solution containing 1,6-dibromohexane (22.40 g, 91.8 mmol) and TPEOH (8.00 g, 23.0 mmol), potassium carbonate powder (6.35 g, 46.0 mmol) was added at room temperature. Then the reaction mixture was gradually heated to 85 °C. After stirring overnight, the mixture was cooled, poured into excess ice-cold water, and extracted with dichloromethane three times. The dichloromethane solution was washed with water and dried

over $MgSO_4$. Following filtration, the solvent was evaporated under vacuum. The resulting crude product was purified by column chromatography on silica gel using *n*-hexane as eluent. EHBr was obtained as a white powder in 73% yield (8.59 g). ^{1}H NMR (300 MHz, $CDCl_3$) δ (ppm): 7.10–6.96 (m, 15H); 6.93–6.86 (d, 2H); 6.63–6.56 (d, 2H); 3.90–3.83 (t, 2H); 3.45–3.33 (t, 2H); 1.98–1.79 (m, 2H); 1.78–1.67 (m, 2H); 1.51–1.42 (m, 4H). ^{13}C NMR (75 MHz, $CDCl_3$) δ (ppm): 157.72, 144.16, 140.74, 140.20, 136.16, 132.67, 131.52, 127.87, 127.75, 126.50, 126.38, 113.79, 67.83, 34.08, 33.04, 29.49, 28.31, 25.69; FT-IR (KBr) ν (cm^{-1}): 3050, 2934, 2860, 1600, 1500, 1445, 1243, 1110, 824, 750, 700, 616; EI-MS, *m*/*z*: $[M]^+$ 510, calcd for $C_{32}H_{31}BrO$ 510; anal. calc. for $C_{32}H_{31}BrO$: C 75.14, H 6.11, Br 15.62, O 3.13; found: C 75.19, H 6.08.

FHE_2Br. To a solution of EHBr (8.44 g, 16.5 mmol), 2-bromo-9*H*-fluorene (2.14 g, 6.6 mmol) and TBAB (0.20 g) in 60 mL of tetrahydrofuran/dimethylsulfoxide (v/v = 1/5), NaOH (w/w 50%, 6.6 mL) was added. The reaction mixture was gradually heated to 60 °C and stirred for 8 h. After workup, the mixture was cooled to room temperature and the solvent was evaporated under vacuum. The residue was added to distilled water, extracted by dichloromethane three times, and dried over $MgSO_4$. Following filtration, the solvent was evaporated under vacuum. The resulting crude product was purified by column chromatography on silica gel using dichloromethane/*n*-hexane (v/v = 1/2) as eluent. FHE_2Br was obtained as a light green powder in 82% yield (5.99 g). ^{1}H NMR (300 MHz, $CDCl_3$) δ (ppm): 7.65–7.60 (m, 1H); 7.44–7.50 (m, 1H); 7.44–7.39 (m, 2H); 7.32–7.27 (m, 3H); 7.14–6.93 (m, 30H); 6.90–6.84 (d, 4H); 6.57–6.51 (d, 4H); 3.77–3.69 (t, 4H); 2.00–1.88 (m, 4H); 1.54–1.47 (m, 4H); 1.21–1.05 (m, 8H); 0.67–0.55(m, 4H). ^{13}C NMR (75 MHz, $CDCl_3$) δ (ppm): 157.32, 152.43, 149.77, 143.74, 140.33, 139.88, 139.70, 135.59, 132.19, 131.10, 129.74, 127.43, 127.31, 126.79, 126.05, 125.93, 125.84, 122.58, 120.83, 120.77, 119.57, 113.32, 67.54, 55.20, 40.12, 29.58, 29.08, 25.62, 23.60; FT-IR (KBr) ν (cm^{-1}): 3052, 2928, 2858, 1600, 1500, 1445, 1240, 1110, 822, 749, 700, 616; FAB-MS, *m*/*z*: $[M + H]^+$ 1107, calcd for $C_{77}H_{69}BrO_2$ 1106; anal. calc. for $C_{77}H_{69}BrO_2$: C 83.60, H 6.29, Br 7.22, O 2.89; found: C 83.56, H 6.32.

FHE_2B. To a degassed solution of FHE_2Br (5.50 g, 4.97 mmol) in 50 mL of 1,4-dioxane, bis(pinacolato)diboron (2.43 g, 9.58 mmol), potassium acetate (1.88 g, 19.16 mmol), and Pd(dppf)Cl_2 (50 mg) were added sequentially. The reaction mixture was gradually heated to 85 °C and stirred overnight. After workup, the mixture was cooled to room temperature and filtered. Following evaporation of solvent under vacuum, the resulting crude product was purified by column chromatography on silica gel using dichloromethane/*n*-hexane (v/v = 1/2) as eluent. FHE_2B was obtained as a light green powder in 85% yield (4.87 g). ^{1}H NMR (300 MHz, $CDCl_3$) δ (ppm): 7.80–7.76 (d, 1H); 7.76–7.65 (t, 3H); 7.32–7.26 (m, 3H); 7.14–6.90 (m, 30H); 6.88–6.83 (d, 4H); 6.56–6.50 (d, 4H); 3.74–3.67 (t, 4H); 2.04–1.92 (m, 4H); 1.54–1.46 (m, 4H); 1.44–1.35 (s, 12H); 1.19–1.03 (m, 8H); 0.65–0.51(m, 4H). ^{13}C NMR (75 MHz, CD_3Cl) δ (ppm): 157.33, 150.77, 149.34, 143.76, 140.66, 140.35, 139.67, 135.54, 133.55, 132.18, 131.11, 128.51, 127.43, 127.31, 126.53, 126.04, 125.93, 122.64, 119.91, 118.78, 113.32, 83.56, 67.56, 54.91, 40.10, 29.65, 29.11, 25.62, 24.92, 23.6 . FT-IR (KBr) ν (cm^{-1}): 3052, 2928, 2855, 1600, 1500, 1353, 1243, 1076, 827, 745, 700; FAB-MS, *m*/*z*: $[M + H]^+$ 1153, calcd for $C_{83}H_{81}BO_4$ 1152; anal. calc. for $C_{83}H_{81}BO_4$: C 86.43, H 7.08, B 0.94, O 5.55; found: C 86.39, H 7.05.

$AF_2H_4E_4$. To a stirring solution of 4-(bis(4-iodophenyl) amino)benzaldehyde (0.68 g, 1.30 mmol) in 50 mL of degassed toluene, FHE_2B (4.50 g, 3.90 mmol), aqueous solution of potassium carbonate (2 M, 9.7 mL, degassed), tetrabutyl ammonium bromide (300 mg), and $Pd(PPh_3)_4$ (50 mg) were added sequentially. The reaction mixture was gradually heated to 85 °C and stirred for 16 h. After workup, the reaction mixture was cooled to room temperature and filtered. Following evaporation of solvent under vacuum, distilled water was added to the residue. The mixture was extracted by chloromethane three times and dried over $MgSO_4$. After filtration and evaporation of solvent, the resulting crude product was purified by column chromatography on silica gel using dichloromethane/*n*-hexane (v/v = 4/5) as eluent. $AF_2H_4E_4$ was obtained as a greenish yellow powder in 71% yield (2.15 g). ^{1}H NMR (300 MHz, $CDCl_3$) δ (ppm): 9.83–9.80 (s, 1H); 7.76–7.49 (m, 16H); 7.35–7.25 (m, 10H); 7.12–6.89 (m, 60H); 6.87–6.82 (d, 8H); 6.55–6.48 (d, 8H); 3.74–3.67 (t, 8H); 2.05–1.96 (m, 8H); 1.52–1.49 (m, 8H); 1.20–1.05 (m, 16H); 0.74–0.62(m, 8H). ^{13}C NMR (75 MHz, $CDCl_3$) δ (ppm): 190.00, 157.28, 152.77, 150.97, 150.38, 144.91, 143.70, 140.28, 139.70, 138.73, 137.97, 135.59, 132.19, 131.09, 128.10, 127.41, 127.31, 126.96, 126.70, 126.06, 125.93, 125.55, 122.60, 120.73, 119.77, 119.58, 113.29, 67.50, 55.00, 40.30, 29.67, 29.08, 25.63, 23.70; FT-IR (KBr) ν (cm^{-1}): 3052, 3020, 2928, 2853, 2725, 1690, 1600, 1500, 1450, 1289, 1242, 1110, 822, 745, 700; FAB-MS, *m*/*z*: $[M + H]^+$ 2324; calcd for $C_{173}H_{151}NO_5$ 2323; anal. calc. for $C_{173}H_{151}NO_5$: C 89.41, H 6.55, N 0.60, O 3.44; found: C 89.38, H 6.57, N 0.58.

AF_2H_4. FHB (5.00 g, 11.25 mmol) and 4-(bis(4-iodophenyl) amino)benzaldehyde (2.44 g, 4.65 mmol) were dissolved in toluene (30 mL), and 2 M aqueous K_2CO_3 solution (28 mL) and TBAB (0.2 g) were added. The mixture was stirred for 40 min under an argon atmosphere at room temperature. Then the $Pd(PPh_3)_4$ (100 mg) was added and the reaction mixture was stirred at 85 °C for 16 h. After cooling to room temperature, the solvent was evaporated and the crude product was purified by silica gel column chromatography using dichloromethane/*n*-hexane (v/v = 1/1) as eluent. A yellow powder was obtained with the yield of 54% (2.35 g). ^{1}H NMR (300 MHz, $CDCl_3$) δ (ppm): 9.88–9.80 (s, 1H); 7.77–7.54 (m, 14H); 7.39–7.27 (m, 10H); 7.23–7.14 (d, 2H); 2.12–1.88 (dd, 8H); 1.16–1.00 (m, 24H); 0.81–0.74 (t, 12H); 0.74–0.56 (m, 8H). ^{13}C NMR (75 MHz, $CDCl_3$) δ (ppm): 190.36, 153.25, 151.66, 151.09, 145.35, 140.84, 140.73, 139.42, 138.60, 131.51, 128.54, 127.00, 125.87, 123.08, 121.31, 120.17, 120.11, 119.93, 55.50, 40.77, 31.83, 30.06, 24.15, 22.91, 14.34. FT-IR (KBr) ν (cm^{-1}): 3060, 3032, 2930, 2856, 1695, 1591, 1509, 1452, 1321, 823, 740. EI-MS, *m*/*z*: 938 $[M]^+$; calcd for $C_{69}H_{79}NO$ 938; anal. calc. for $C_{69}H_{79}NO$: C 88.32, H 8.49, N1.49, O 1.71; found: C 88.30, H 8.51, N1.47.

$PA_2F_4H_8E_8$. To a stirring solution of anhydrous tetrahydrofuran (20 mL) containing 1,4-bis(diethylphosphorylmethyl) benzene ($Bpho_2$, 0.07 g, 0.19 mmol) and $AF_2H_4E_4$ (0.90 g, 0.39 mmol) was added potassium *tert*-butoxide (0.09 g, 0.80 mmol) at

room temperature. The reaction mixture was stirring for 30 min. After workup, a substantial amount of ethanol was added to the reaction mixture to obtain a light green precipitation. Following filtration, the resulting crude product was purified by column chromatography on silica gel using dichloromethane/*n*-hexane (v/v = 1/2) as eluent. $PA_2F_4H_8E_8$ was obtained as a light green powder in 88% yield (0.79 g). ^{1}H NMR (300 MHz, $CDCl_3$) δ (ppm): 7.72–7.65 (t, 9H); 7.61–7.50 (m, 18H); 7.46–7.39 (d, 9H); 7.34–7.25 (m, 15H); 7.22–7.21 (s, 3H); 7.19–7.13 (d, 6H); 7.12–6.92 (m, 120H); 6.89–6.80 (d, 16H); 6.55–6.47 (d, 16H); 3.74–3.65 (t, 16H); 2.06–1.93 (m, 16H); 1.52–1.46 (m, 16H); 1.21–1.08 (m, 32H); 0.74–0.62 (m, 16H). ^{13}C NMR (75 MHz, $CDCl_3$) δ (ppm): 157.75, 151.33, 150.82, 144.18, 140.98, 140.76, 140.35, 140.12, 139.54, 136.02, 132.69, 131.56, 127.79, 126.42, 125.85, 124.86, 123.05, 121.03, 120.23, 119.97, 113.79, 67.96, 55.43, 40.77, 30.13, 29.54, 26.08, 24.15; FT-IR (KBr) ν (cm^{-1}): 3050, 3026, 2928, 2853, 1600, 1500, 1450, 1290, 1243, 1110, 824, 745, 700; MALDI TOF-MS, *m*/*z*: $[M]^+$ 4718; calcd for $C_{354}H_{308}N_2O_8$ 4718; anal. calc. for $C_{354}H_{308}N_2O_8$: C 90.11, H 6.58, N 0.59, O 2.71; found: C 90.14, H 6.60, N 0.56.

$PA_2F_4H_8$. The synthesis of $PA_2F_4H_8$ was similar to $PA_2F_4H_8E_8$. $PA_2F_4H_8$ was obtained as a yellow green powder in 89% yield (0.47 g). ^{1}H NMR (300 MHz, $CDCl_3$) δ (ppm): 7.78–7.68 (t, 8H); 7.68–7.48 (dd, 22H); 7.48–7.42 (d, 4H); 7.37–7.26 (m, 18H); 7.22–7.16 (d, 4H); 7.13–7.01 (d, 4H); 2.07–1.94 (dd, 16H); 1.16–1.02 (m, 48H); 0.80–0.74 (t, 24H); 0.74–0.64 (m, 16H). ^{13}C NMR (75 MHz, $CDCl_3$) δ (ppm): 151.11, 150.63, 146.72, 146.23, 140.51, 149.87, 139.03, 137.95, 136.44, 136.04, 131.69, 127.67, 127.21, 126.69, 126.51, 126.43, 125.25, 124.37, 123.69, 122.61, 120.69, 119.69, 119.42, 55.01, 40.38, 31.43, 29.67, 23.71, 22.54, 13.98. FT-IR (KBr) ν (cm^{-1}): 3060, 3031, 2926, 2853, 1597, 1511, 1452, 1321, 823, 741. FAB-MS, *m*/*z*: $[M + H]^+$ 1946; calcd for $C_{146}H_{164}N_2$ 1945; anal. calc. for $C_{146}H_{164}N_2$: C 90.07, H 8.49, N 1.44; found: C 90.01, H 8.46, N 1.42.

$AnA_2F_4H_8E_8$. The synthesis of $AnA_2F_4H_8E_8$ was similar to $PA_2F_4H_8E_8$. $AnA_2F_4H_8E_8$ was obtained as a yellow powder in 84% yield (0.77 g). ^{1}H NMR (300 MHz, $CDCl_3$) δ (ppm): 7.44–7.37 (s, 4H); 7.89–7.52 (m, 36H); 7.47–7.42 (m, 4H); 7.34–7.26 (m, 20H); 7.14–6.90 (m, 120H); 6.89–6.82 (d, 16H); 6.56–6.47 (d, 16H); 3.75–3.65 (t, 16H); 2.07–1.95 (m, 16H); 1.53–1.47 (m, 16H); 1.23–1.08 (m, 32H); 0.74–0.62 (m, 16H). ^{13}C NMR (75 MHz, $CDCl_3$) δ (ppm): 157.74, 151.34, 150.81, 146.74, 144.20, 144.15, 140.97, 140.74, 140.35, 140.11, 139.55, 136.43, 136.00, 132.62, 131.53, 129.86, 128.17, 127.10, 126.48, 126.36, 125.83, 125.39, 124.81, 123.03, 121.04, 120.22, 119.94, 113.74, 67.95, 55.42, 40.76, 30.12, 29.52, 26.07, 24.15; FT-IR (KBr) ν (cm^{-1}): 3050, 3026, 2928, 2853, 1600, 1500, 1450, 1290, 1243, 1110, 821, 745, 700; MALDI TOF-MS, *m*/*z*: $[M]^+$ 4818; calcd for $C_{362}H_{312}N_2O_8$ 4818; anal. calc. for $C_{362}H_{312}N_2O_8$: C 90.24, H 6.53, N 0.58, O 2.66; found: C 90.21, H 6.54, N 0.60.

$AnA_2F_4H_8$. The synthesis of $AnA_2F_4H_8$ was similar to $PA_2F_4H_8E_8$. $AnA_2F_4H_8$ was obtained as a yellow powder in 72% yield (0.38 g). ^{1}H NMR (300 MHz, $CDCl_3$) δ (ppm): 8.48–8.49 (m, 4H); 7.95–7.78 (d, 2H); 7.77–7.70 (m, 8H); 7.66–7.57 (m, 20H); 7.52–7.47 (dd, 4H); 7.36–7.28 (m, 24H); 6.98–6.89 (d, 2H); 2.07–1.96 (dd, 16H); 1.15–1.03 (m, 48H); 0.82–0.76 (t, 24H); 0.74–0.64 (m, 16H). ^{13}C NMR (75 MHz, $CDCl_3$) δ (ppm): 151.60, 151.10, 147.62, 146.75, 140.98, 140.36, 139.54, 137.06, 136.62, 132.97, 132.18, 129.90, 128.19, 127.78, 126.97, 126.76, 125.73, 125.37, 124.84, 123.88, 123.07, 121.20, 120.13, 119.87, 55.48, 40.81, 31.86, 30.10, 24.18, 22.94, 14.37. FT-IR (KBr) ν (cm^{-1}): 3060, 3030, 2926, 2851, 1600, 1508, 1450, 1321, 820, 737. MALDI TOF-MS, *m*/*z*: $[M]^+$ 2047.8; calcd for $C_{154}H_{168}N_2$ 2047; anal. calc. for $C_{154}H_{168}N_2$: C 90.36, H 8.27, N 1.37; found: C 90.31, H 8.30, N 1.39.

Acknowledgements

The authors gratefully acknowledge the financial support from the NSF of China (51173210, 51073177), the Fundamental Research Funds for the Central Universities and NSF of Guangdong (S2011020001190).

Notes and references

1 N. Y. Baek, C. H. Heo, C. S. Lim, G. Masanta, B. R. Cho and H. M. Kim, *Chem. Commun.*, 2012, **48**, 4546.
2 G. Masanta, C. S. Lim, H. J. Kim, J. H. Han, H. M. Kim and B. R. Cho, *J. Am. Chem. Soc.*, 2011, **133**, 5698–5700.
3 J. H. Lee, C. S. Lim, Y. S. Tian, J. H. Han and B. R. Cho, *J. Am. Chem. Soc.*, 2010, **132**, 1216–1217.
4 H. M. Kim, M. S. Seo, M. J. An, J. H. Hong, Y. S. Tian, J. H. Choi, O. Kwon, K. J. Lee and B. R. Cho, *Angew. Chem., Int. Ed.*, 2008, **47**, 5167–5170.
5 M. Taki, J. L. Wolford and T. V. O'Halloran, *J. Am. Chem. Soc.*, 2004, **126**, 712–713.
6 K.-Y. Pu, K. Li, X. Zhang and B. Liu, *Adv. Mater.*, 2010, **22**, 4186–4189.
7 M. Q. Zhu, G. F. Zhang, C. Li, M. P. Aldred, E. Chang, R. A. Drezek and A. D. Q. Li, *J. Am. Chem. Soc.*, 2011, **133**, 365–372.
8 J. Lott, C. Ryan, B. Valle, J. R. Johnson III, D. A. Schiraldi, J. Shan, K. D. Singer and C. Weder, *Adv. Mater.*, 2011, **23**, 2425–2429.
9 A. Royon, K. Bourhis, M. Bellec, G. Papon, B. Bousquet, Y. Deshayes, T. Cardinal and L. Canioni, *Adv. Mater.*, 2010, **22**, 5282–5286.
10 C. C. Corredor, Z. L. Huang and K. D. Belfield, *Adv. Mater.*, 2006, **18**, 2910–2914.
11 S. Sumalekshmy and C. J. Fahrni, *Chem. Mater.*, 2011, **23**, 483–500.
12 W. R. Zipfel, R. M. Williams and W. W. Webb, *Nat. Biotechnol.*, 2003, **21**, 1369–1377.
13 N. A. A. Rahim, W. McDaniel, K. Bardon, S. Srinivasan, V. Vickerman, P. T. C. So and J. H. Moon, *Adv. Mater.*, 2009, **21**, 3492–3496.
14 C. Xu, W. Zipfel, J. B. Shear, R. M. Williams and A. W. W. Webb, *Proc. Natl. Acad. Sci. U. S. A.*, 1996, **93**, 10763–10768.
15 W. J. Yang, C. H. Kim, M. Y. Jeong, S. K. Lee, M. J. Piao, S. J. Jeon and B. R. Cho, *Chem. Mater.*, 2004, **16**, 2783–2789.
16 R. Kannan, G. S. He, L. Yuan, F. Xu, P. N. Prasad, A. G. Dombroskie, B. A. Reinhardt, J. W. Baur, R. A. Vaia and L. S. Tan, *Chem. Mater.*, 2001, **13**, 1896–1904.

17 Z. Q. Liu, Q. Fang, D. X. Cao, D. Wang and G. B. Xu, *Org. Lett.*, 2004, **6**, 2933–2936.
18 M. Rumi, J. E. Ehrlich, A. A. Heikal, J. W. Perry, S. Barlow, Z. Hu, D. McCord-Maughon, T. C. Parker, H. Röckel, S. Thayumanavan, S. R. Marder, D. Beljonne and J. L. Brédas, *J. Am. Chem. Soc.*, 2000, **122**, 9500–9510.
19 G. S. He, L. S. Tan, Q. Zheng and P. N. Prasad, *Chem. Rev.*, 2008, **108**, 1245–1330.
20 S. J. K. Pond, M. Rumi, M. D. Levin, T. C. Parker, D. Beljonne, M. W. Day, J. L. Brédas, S. R. Marder and J. W. Perry, *J. Phys. Chem. A*, 2002, **106**, 11470–11480.
21 K. R. J. Thomas, J. T. Lin, Y. C. Hsu and K. C. Ho, *Chem. Commun.*, 2005, 4098.
22 S. J. Chung, S. Zheng, T. Odani, L. Beverina, J. Fu, L. A. Padilha, A. Biesso, J. M. Hales, X. Zhan, K. Schmidt, A. Ye, E. Zojer, S. Barlow, D. J. Hagan, E. W. Van Stryland, Y. Yi, Z. Shuai, G. A. Pagani, J. L. Brédas, J. W. Perry and S. R. Marder, *J. Am. Chem. Soc.*, 2006, **128**, 14444–14445.
23 L. Beverina, J. Fu, A. Leclercq, E. Zojer, P. Pacher, S. Barlow, E. W. Van Stryland, D. J. Hagan, J. L. Brédas and S. R. Marder, *J. Am. Chem. Soc.*, 2005, **127**, 7282–7283.
24 A. R. Morales, K. D. Belfield, J. M. Hales, E. W. Van Stryland and D. J. Hagan, *Chem. Mater.*, 2006, **18**, 4972–4980.
25 K. D. Belfield, D. J. Hagan, E. W. Van Stryland, K. J. Schafer and R. A. Negres, *Org. Lett.*, 1999, **1**, 1575–1578.
26 M. Pawlicki, H. A. Collins, R. G. Denning and H. L. Anderson, *Angew. Chem., Int. Ed.*, 2009, **48**, 3244–3266.
27 M. Albota, *Science*, 1998, **281**, 1653–1656.
28 S. Kawata and Y. Kawata, *Chem. Rev.*, 2000, **100**, 1777–1788.
29 Y. Hai, J. J. Chen, P. Zhao, H. Lv, Y. Yu, P. Xu and J. L. Zhang, *Chem. Commun.*, 2011, **47**, 2435.
30 B. Strehmel, A. M. Sarker, J. H. Malpert, V. Strehmel, H. Seifert and D. C. Neckers, *J. Am. Chem. Soc.*, 1999, **121**, 1226–1236.
31 H. Y. Woo, J. W. Hong, B. Liu, A. Mikhailovsky, D. Korystov and G. C. Bazan, *J. Am. Chem. Soc.*, 2005, **127**, 820–821.
32 Z. Xu, Q. Liao, Y. Wu, W. Ren, W. Li, L. Liu, S. Wang, Z. Gu, H. Zhang and H. Fu, *J. Mater. Chem.*, 2012, **22**, 17737.
33 M. Velusamy, J. Y. Shen, J. T. Lin, Y. C. Lin, C. C. Hsieh, C. H. Lai, C. W. Lai, M. L. Ho, Y. C. Chen, P. T. Chou and J. K. Hsiao, *Adv. Funct. Mater.*, 2009, **19**, 2388–2397.
34 A. Burns, H. Ow and U. Wiesner, *Chem. Soc. Rev.*, 2006, **35**, 1028.
35 R. Jakubiak, C. J. Collison, W. C. Wan, L. J. Rothberg and B. R. Hsieh, *J. Phys.Chem. A*, 1999, **103**, 2394–2398.
36 M. Grell, D. D. C. Bradley, G. Ungar, J. Hill and K. S. Whitehead, *Macromolecules*, 1999, **32**, 5810–5817.
37 S. W. Thomas, G. D. Joly and T. M. Swager, *Chem. Rev.*, 2007, **107**, 1339–1386.
38 J. Luo, Z. Xie, J. W. Y. Lam, L. Cheng, B. Z. Tang, H. Chen, C. Qiu, H. S. Kwok, X. Zhan, Y. Liu and D. Zhu, *Chem. Commun.*, 2001, 1740–1741.
39 Y. Hong, J. W. Y. Lam and B. Z. Tang, *Chem. Soc. Rev.*, 2011, **40**, 5361.
40 Y. Hong, J. W. Y. Lam and B. Z. Tang, *Chem. Commun.*, 2009, 4332.
41 Z. Zhao, S. Chen, J. W. Y. Lam, P. Lu, Y. Zhong, K. S. Wong, H. S. Kwok and B. Z. Tang, *Chem. Commun.*, 2010, **46**, 2221.
42 B. K. An, S. K. Kwon, S. D. Jung and S. Y. Park, *J. Am. Chem. Soc.*, 2002, **124**, 14410–14415.
43 W. Z. Yuan, P. Lu, S. Chen, J. W. Y. Lam, Z. Wang, Y. Liu, H. S. Kwok, Y. Ma and B. Z. Tang, *Adv. Mater.*, 2010, **22**, 2159–2163.
44 Z. Zhao, P. Lu, J. W. Y. Lam, Z. Wang, C. Y. K. Chan, H. H. Y. Sung, I. D. Williams, Y. Ma and B. Z. Tang, *Chem. Sci.*, 2011, **2**, 672.
45 B. Xu, M. Xie, J. He, B. Xu, Z. Chi, W. Tian, L. Jiang, F. Zhao, S. Liu, Y. Zhang, Z. Xu and J. Xu, *Chem. Commun.*, 2013, **49**, 273.
46 B. Xu, Z. Chi, J. Zhang, X. Zhang, H. Li, X. Li, S. Liu, Y. Zhang and J. Xu, *Chem.–Asian J.*, 2011, **6**, 1470–1478.
47 Z. Yang, Z. Chi, B. Xu, H. Li, X. Zhang, X. Li, S. Liu, Y. Zhang and J. Xu, *J. Mater. Chem.*, 2010, **20**, 7352.
48 N. Mataga, Y. Kaifu and M. Koizumi, *Bull. Chem. Soc. Jpn.*, 1956, **29**, 465.
49 Y. Jiang, Y. Wang, J. Hua, J. Tang, B. Li, S. Qian and H. Tian, *Chem. Commun.*, 2010, **46**, 4689.
50 Q. Zheng, G. S. He, C. Lu and P. N. Prasad, *J. Mater. Chem.*, 2005, **15**, 3488.
51 Q. Zheng, S. K. Gupta, G. S. He, L. S. Tan and P. N. Prasad, *Adv. Funct. Mater.*, 2008, **18**, 2770–2779.
52 R. D. Hreha, C. P. George, A. Haldi, B. Domercq, M. Malagoli, S. Barlow, J. L. Brédas, B. Kippelen and S. R. Marder, *Adv. Funct. Mater.*, 2003, **13**, 967–973.
53 M. Kimura, S. Kuwano, Y. Sawaki, H. Fujikawa, K. Noda, Y. Taga and K. Takagi, *J. Mater. Chem.*, 2005, **15**, 2393.
54 H. Tong, Y. Hong, Y. Dong, M. Haussler, J. W. Y. Lam, Z. Li, Z. Guo, Z. Guo and B. Z. Tang, *Chem. Commun.*, 2006, 3705.
55 W. Y. Wong, G. J. Zhou, X. M. Yu, H. S. Kwok and B. Z. Tang, *Adv. Funct. Mater.*, 2006, **16**, 838–846.
56 Y. Wang, T. Liu, L. Bu, J. Li, C. Yang, X. Li, Y. Tao and W. Yang, *J. Phys. Chem. C*, 2012, **116**, 15576–15583.
57 W. Z. Yuan, Y. Gong, S. Chen, X. Y. Shen, J. W. Y. Lam, P. Lu, Y. Lu, Z. Wang, R. Hu, N. Xie, H. S. Kwok, Y. Zhang, J. Z. Sun and B. Z. Tang, *Chem. Mater.*, 2012, **24**, 1518–1528.
58 Y. Zhao, A. M. Ren, J. K. Feng, X. Zhou, X. C. Ai and W. J. Su, *Phys. Chem. Chem. Phys.*, 2009, **11**, 11538.
59 W. Wang, T. Lin, M. Wang, T. X. Liu, L. Ren, D. Chen and S. Huang, *J. Phys. Chem. B*, 2010, **114**, 5983–5988.
60 Q. Chen, D. Zhang, G. Zhang, X. Yang, Y. Feng, Q. Fan and D. Zhu, *Adv. Funct. Mater.*, 2010, **20**, 3244–3251.
61 B. Z. Tang, Y. Geng, J. W. Y. Lam, B. Li, X. Jing, X. Wang, F. Wang, A. B. Pakhomov and X. X. Zhang, *Chem. Mater.*, 1999, **11**, 1581–1589.
62 B. Li, R. Tong, R. Zhu, F. Meng, H. Tian and S. Qian, *J. Phys. Chem. B*, 2005, **109**, 10705–10710.
63 Y. Jiang, Y. Wang, J. Hua, S. Qu, S. Qian and H. Tian, *J. Polym. Sci., Part A: Polym. Chem.*, 2009, **47**, 4400–4408.
64 Y. Wu, X. Shen, S. Dai, Y. Xu, F. Chen, C. Lin, T. Xu and Q. Nie, *J. Phys. Chem. C*, 2011, **115**, 25040–25045.
65 E. Q. Guo, P. H. Ren, Y. L. Zhang, H. C. Zhang and W. J. Yang, *Chem. Commun.*, 2009, 5859.
66 H. C. Zhang, E. Q. Guo, Y. L. Zhang, P. H. Ren and W. J. Yang, *Chem. Mater.*, 2009, **21**, 5125–5135.

67 S. Kim, Q. Zheng, G. S. He, D. J. Bharali, H. E. Pudavar, A. Baev and P. N. Prasad, *Adv. Funct. Mater.*, 2006, **16**, 2317–2323.
68 S. Kim, H. E. Pudavar, A. Bonoiu and P. N. Prasad, *Adv. Mater.*, 2007, **19**, 3791–3795.
69 F. He, L. L. Tian, X. Y. Tian, H. Xu, Y. H. Wang, W. J. Xie, M. Hanif, J. L. Xia, F. Z. Shen, B. Yang, F. Li, Y. G. Ma, Y. Q. Yang and J. C. Shen, *Adv. Funct. Mater.*, 2007, **17**, 1551–1557.
70 F. Gao, Q. Liao, Z. Z. Xu, Y. H. Yue, Q. Wang, H. L. Zhang and H. B. Fu, *Angew. Chem., Int. Ed.*, 2010, **49**, 732–735.
71 J. Daub, R. Engl, J. Kurzawa, S. E. Miller, S. Schneider, A. Stockmann and M. R. Wasielewski, *J. Phys. Chem. A*, 2001, **105**, 5655–5665.
72 Y. Li, T. Ren and W. J. Dong, *J. Photochem. Photobiol., A*, 2013, **251**, 1–9.
73 K. Podgorski, E. Terpetschnig, O. P. Klochko, O. M. Obukhova and K. Haas, *PLoS One*, 2012, **7**, e51980.
74 X. Wang, X. Tian, Q. Zhang, P. Sun, J. Wu, H. Zhou, B. Jin, J. Yang, S. Zhang, C. Wang, X. Tao, M. Jiang and Y. Tian, *Chem. Mater.*, 2012, **24**, 954–961.
75 B. Wang, Y. Wang, J. Hua, Y. Jiang, J. Huang, S. Qian and H. Tian, *Chem.–Eur. J.*, 2011, **17**, 2647–2655.
76 S. Ye, Y. Liu, J. Chen, K. Lu, W. Wu, C. Du, Y. Liu, T. Wu, Z. Shuai and G. Yu, *Adv. Mater.*, 2010, **22**, 4167–4171.
77 N. Metri, X. Sallenave, C. Plesse, L. Beouch, P. H. Aubert, F. Goubard, C. Chevrot and G. Sini, *J. Phys. Chem. C*, 2012, **116**, 3765–3772.
78 P. I. Shih, C. Y. Chuang, C. H. Chien, E. W. G. Diau and C. F. Shu, *Adv. Funct. Mater.*, 2007, **17**, 3141–3146.
79 A. Winter, C. Friebe, M. D. Hager and U. S. Schubert, *Eur. J. Org. Chem.*, 2009, 801–809.
80 Z. Wang, P. Lu, S. Xue, C. Gu, Y. Lv, Q. Zhu, H. Wang and Y. Ma, *Dyes Pigm.*, 2011, **91**, 356–363.
81 M. Sheikbahae, A. A. Said, T. H. Wei, D. J. Hagan and E. W. Vanstryland, *IEEE J. Quantum Electron.*, 1990, **26**, 760–769.

